

# PAMELA results on the cosmic-ray antiproton flux

O. Adriani,<sup>1,2</sup> G. C. Barbarino,<sup>3,4</sup> G. A. Bazilevskaya,<sup>5</sup> R. Bellotti,<sup>6,7</sup> M. Boezio,<sup>8</sup> E. A. Bogomolov,<sup>9</sup> L. Bonechi,<sup>1,2</sup> M. Bongi,<sup>2</sup> V. Bonvicini,<sup>8</sup> S. Borisov,<sup>10,11,12</sup> S. Bottai,<sup>2</sup> A. Bruno,<sup>6,7</sup> F. Cafagna,<sup>7</sup> D. Campana,<sup>4</sup> R. Carbone,<sup>4,11</sup> P. Carlson,<sup>13</sup> M. Casolino,<sup>10</sup> G. Castellini,<sup>14</sup> L. Consiglio,<sup>4</sup> M. P. De Pascale,<sup>10,11</sup> C. De Santis,<sup>10</sup> N. De Simone,<sup>10,11</sup> V. Di Felice,<sup>10,11</sup> A. M. Galper,<sup>12</sup> W. Gillard,<sup>13</sup> L. Grishantseva,<sup>12</sup> P. Hofverberg,<sup>13</sup> G. Jerse,<sup>8,15</sup> A. V. Karelin,<sup>12</sup> S. V. Koldashov,<sup>12</sup> S. Y. Krutkov,<sup>9</sup> A. N. Kvashnin,<sup>5</sup> A. Leonov,<sup>12</sup> V. Malvezzi,<sup>10</sup> L. Marcelli,<sup>10</sup> A. G. Mayorov,<sup>12</sup> W. Menn,<sup>16</sup> V. V. Mikhailov,<sup>12</sup> E. Mocchiutti,<sup>8</sup> A. Monaco,<sup>6,7</sup> N. Mori,<sup>2</sup> N. Nikonov,<sup>9,10,11</sup> G. Osteria,<sup>4</sup> P. Papini,<sup>2</sup> M. Pearce,<sup>13</sup> P. Picozza,<sup>10,11</sup> C. Pizzolotto,<sup>8</sup> M. Ricci,<sup>17</sup> S. B. Ricciarini,<sup>2</sup> L. Rossetto,<sup>13</sup> M. Simon,<sup>16</sup> R. Sparvoli,<sup>10,11</sup> P. Spillantini,<sup>1,2</sup> Y. I. Stozhkov,<sup>5</sup> A. Vacchi,<sup>8</sup> E. Vannuccini,<sup>2</sup> G. Vasilyev,<sup>9</sup> S. A. Voronov,<sup>12</sup> J. Wu,<sup>13,\*</sup> Y. T. Yurkin,<sup>12</sup> G. Zampa,<sup>8</sup> N. Zampa,<sup>8</sup> and V. G. Zverev<sup>12</sup>

<sup>1</sup>*University of Florence, Department of Physics,  
I-50019 Sesto Fiorentino, Florence, Italy*

<sup>2</sup>*INFN, Sezione di Florence, I-50019 Sesto Fiorentino, Florence, Italy*

<sup>3</sup>*University of Naples “Federico II”,  
Department of Physics, I-80126 Naples, Italy*

<sup>4</sup>*INFN, Sezione di Naples, I-80126 Naples, Italy*

<sup>5</sup>*Lebedev Physical Institute, RU-119991 Moscow, Russia*

<sup>6</sup>*University of Bari, Department of Physics, I-70126 Bari, Italy*

<sup>7</sup>*INFN, Sezione di Bari, I-70126 Bari, Italy*

<sup>8</sup>*INFN, Sezione di Trieste, I-34149 Trieste, Italy*

<sup>9</sup>*Ioffe Physical Technical Institute, RU-194021 St. Petersburg, Russia*

<sup>10</sup>*INFN, Sezione di Rome “Tor Vergata”, I-00133 Rome, Italy*

<sup>11</sup>*University of Rome “Tor Vergata”,*

*Department of Physics, I-00133 Rome, Italy*

<sup>12</sup>*Moscow Engineering and Physics Institute, RU-11540 Moscow, Russia*

<sup>13</sup>*KTH, Department of Physics, and the Oskar Klein Centre for Cosmoparticle Physics,  
AlbaNova University Centre, SE-10691 Stockholm, Sweden*

<sup>14</sup>*IFAC, I-50019 Sesto Fiorentino, Florence, Italy*

<sup>15</sup>*University of Trieste, Department of Physics, I-34147 Trieste, Italy*  
<sup>16</sup>*Universität Siegen, Department of Physics, D-57068 Siegen, Germany*

<sup>17</sup>*INFN, Laboratori Nazionali di Frascati,  
Via Enrico Fermi 40, I-00044 Frascati, Italy*

(Dated: November 4, 2018)

## Abstract

The satellite-borne experiment PAMELA has been used to make a new measurement of the cosmic-ray antiproton flux and the antiproton-to-proton flux ratio which extends previously published measurements down to 60 MeV and up to 180 GeV in kinetic energy. During 850 days of data acquisition approximately 1500 antiprotons were observed. The measurements are consistent with purely secondary production of antiprotons in the galaxy. More precise secondary production models are required for a complete interpretation of the results.

PACS numbers: 96.50.sb, 95.35.+d, 95.55.Vj

Antiprotons and positrons are a small but not negligible component of the cosmic radiation. They can be produced in the interactions between cosmic-ray nuclei and the interstellar matter. Detailed measurements of the cosmic-ray antiproton energy spectrum therefore provide important information concerning the origin and propagation of cosmic-rays. Exotic sources of primary antiprotons such as the annihilation of dark matter particles [1–3] and the evaporation of primordial black holes [4, 5] can also be probed. The theoretical energy spectrum of secondary antiprotons has a distinct peak around 2 GeV and rapidly decreases towards lower energies due to the kinematic constraints on the antiproton production. At higher energies the spectrum is slightly steeper than that of the parent protons (e.g. see [6]), which results in a slight decrease of the antiproton-to-proton flux ratio.

Since July 2006, PAMELA (a Payload for Antimatter Matter Exploration and Light-nuclei Astrophysics) is measuring the antiparticle component of the cosmic radiation. A previous PAMELA measurement of the antiproton-to-proton flux ratio between 1.5 and 100 GeV [7], was found to follow the expectation from secondary production calculations. However, the positron fraction [8, 9] measured in the same energy range showed a clear deviation from secondary production models. In order to explain these results both astrophysical objects (e.g. pulsars) and dark matter have been proposed as positron sources (e.g. [10]). A contribution from pulsars would naturally increase the positron and electron abundances without affecting the antiproton component. Other astrophysical models [11] have been proposed to explain the PAMELA positron results but produce an increase in the antiproton component at very high energies ( $\geq 100$  GeV). A dark matter contribution may require pure leptonic annihilation channels, e.g. [12], or the introduction of a new dark sector of forces, e.g. [13]. In [14] it is noted that any signal in the antiproton energy spectrum may be hidden due to incomplete modelling of secondary production and cosmic-ray propagation. A detailed measurement of the antiproton energy spectrum over a large energy range is therefore of great interest.

The PAMELA experiment [10, 15] comprises (from top to bottom): a time of flight system, a magnetic spectrometer with silicon tracker planes, an anticoincidence system, an electromagnetic imaging calorimeter, a shower tail catcher scintillator and a neutron detector. These components are housed inside a pressurized container attached to the Russian Resurs-DK1 satellite, which was launched on June 15<sup>th</sup> 2006. The orbit is elliptical and semi-polar, with an inclination of  $70.0^\circ$  and an altitude varying between 350 km and

610 km.

We report on the cosmic-ray antiproton flux over the widest energy range ever achieved: 60 MeV to 180 GeV. We also confirm and extend the previously published PAMELA antiproton-to-proton flux ratio measurement [7] to the same energy range. Data were acquired from July 2006 to December 2008 (850 days), corresponding to  $> 10^9$  triggers. Triggered events were selected for analysis if the reconstructed rigidity exceeded the vertical geomagnetic cut-off (estimated using the satellite orbital information) by a factor of 1.3. Downward-going charge-one particles were selected using the time-of-flight and spectrometer data. Time-of-flight information was also used to select low velocity (anti)protons while electrons were rejected using the electromagnetic calorimeter information, as described in [7]. The remaining electron contamination was estimated to be negligible while contamination from locally produced pions was found to be about 10% between 1 and 3 GV/c and negligible at lower and higher rigidities [7, 16].

The highest energy at which antiprotons can be unambiguously measured by PAMELA is determined by the contamination of “spillover” protons which are reconstructed with an incorrect sign of curvature either due to the finite spectrometer resolution or scattering in the spectrometer planes. To reduce this contamination, strict requirements were applied on the quality of the tracks reconstructed in the spectrometer. For example, tracks accompanied by  $\delta$ -ray emission were discarded to avoid poorly reconstructed coordinates on the silicon planes of the spectrometer. For each track the maximum detectable rigidity (MDR) was evaluated on an event-by-event basis by propagating the estimated coordinate errors and taking into account the track topology. The MDR was required to be 6 times larger than the measured rigidity. This allowed the antiproton measurement to be extended up to 180 GV/c with acceptable contamination from spillover protons. The contamination was estimated using the GPAMELA detector simulation which is based on the GEANT3 package [17]. The simulation contains an accurate representation of the geometry and performance of the PAMELA detectors. For the spectrometer [18] the measured noise of each silicon plane and performance variations over the duration of the measurement were accounted for. The simulation code was validated by comparing the distributions of several significant variables (e.g. coordinate residuals,  $\chi^2$  and the covariance matrix from the track fitting) with those obtained from real data. The high-energy region of the deflection distribution was studied before applying the MDR selection and agreement within 20% was found between data

and simulation. This difference was taken as a systematic uncertainty on the spillover contamination which was estimated to be  $\simeq 30\%$  for the rigidity interval 100-180 GV/c.

The efficiencies were carefully studied using both experimental and simulated data [16, 19, 20]. The time dependence of the detector performance (and therefore also efficiency) was studied using proton samples collected during 2 month long periods. The average global selection efficiency was measured to be  $\simeq 30\%$ . The number of (anti)protons rejected by the selection criteria due to interactions and energy loss within the detector systems was estimated using the simulation. The number of antiprotons lost due to this selection is energy dependent and varies from  $\simeq 10\%$  below 1 GeV to  $\simeq 6\%$  above 50 GeV. The antiproton flux was obtained by considering the geometrical factor (estimated both analytically and with simulations) and the total live time which is provided by an on-board clock that times the periods during which the apparatus is waiting for a trigger.

The energy-binned antiproton fluxes and antiproton-to-proton flux ratios are given in Table I. The spectrometer resolution has not been unfolded and a systematic uncertainty is included to account for this. Contamination from pions and spillover protons has been subtracted from the results. The first and second errors in the table represent the statistical and systematic uncertainties, respectively. The total systematic uncertainty was obtained quadratically summing the various systematic errors considered: acceptance, contamination, efficiency estimation, energy losses, interactions and spectrum unfolding.

Figure 1 shows the antiproton energy spectrum and Figure 2 shows the antiproton-to-proton flux ratio measured by PAMELA along with other recent experimental data [21–25, 28] and theoretical calculations assuming pure secondary production of antiprotons during the propagation of cosmic rays in the galaxy. The curves were calculated for solar minimum, which is appropriate for the PAMELA data taking period, using the force field approximation [29], [37].

The PAMELA results reproduce the expected peak around 2 GeV in the antiproton flux and are in overall agreement with pure secondary calculations. The experimental uncertainties are smaller than the spread in the different theoretical curves and, therefore, provide important constraints on parameters relevant for secondary production calculations. For example, the antiproton flux bands from Donato et al. [26] presented in Figure 1 show uncertainties on the propagation parameters (dotted lines) and antiproton production cross-sections (dashed lines) and indicate larger uncertainties than those present in the PAMELA

TABLE I: Summary of antiproton results. Antiproton fluxes ( $\times 10^{-3}$  particles/( $\text{m}^2 \text{ sr s GeV}$ )) and antiproton-to-proton flux ratios ( $\times 10^{-5}$ ). The upper limits are 90% confidence levels. The first and second errors represent the statistical and systematic uncertainties, respectively.

| Rigidity<br>at the<br>spectrometer<br>GV/c | Mean Kinetic<br>Energy at<br>top of<br>payload GeV | Observed<br>number of<br>events $\bar{p}$ | Flux<br>at top of<br>payload            | $\frac{\bar{p}}{p}$<br>at top of<br>payload |
|--|--|---|---|---|
| 0.35 - 0.50                                | 0.09   | 0   | < 6.4                                   | < 0.73                                      |
| 0.50 - 1.01                                | 0.28   | 7   | $6.7 \pm 2.7 \pm 0.2$                   | $0.48 \pm 0.18 \pm 0.01$                    |
| 1.01 - 1.34                                | 0.56   | 15  | $15.3^{+7.5}_{-3.7} \pm 0.9$            | $0.99^{+0.31}_{-0.26} \pm 0.07$             |
| 1.34 - 1.63                                | 0.81   | 19  | $17.2^{+7.4}_{-3.9} \pm 1.1$            | $1.33^{+0.38}_{-0.33} \pm 0.10$             |
| 1.63 - 1.93                                | 1.07   | 32  | $21.4^{+6.8}_{-3.9} \pm 1.3$            | $2.04 \pm 0.44 \pm 0.15$                    |
| 1.93 - 2.23                                | 1.34   | 39  | $24.5^{+7.2}_{-4.3} \pm 1.5$            | $2.78 \pm 0.54 \pm 0.20$                    |
| 2.23 - 2.58                                | 1.61   | 49  | $20.5 \pm 3.2 \pm 1.2$                  | $3.43 \pm 0.49 \pm 0.24$                    |
| 2.58 - 2.99                                | 2.03   | 78  | $27.1 \pm 3.3 \pm 1.6$                  | $5.44 \pm 0.62 \pm 0.39$                    |
| 2.99 - 3.45                                | 2.42   | 79  | $21.9 \pm 2.6 \pm 1.3$                  | $6.10 \pm 0.68 \pm 0.43$                    |
| 3.45 - 3.99                                | 2.90   | 96  | $22.7 \pm 2.5 \pm 1.3$                  | $7.78 \pm 0.79 \pm 0.55$                    |
| 3.99 - 4.62                                | 3.47   | 103                                       | $17.8 \pm 1.9 \pm 1.0$                  | $9.15 \pm 0.89 \pm 0.65$                    |
| 4.62 - 5.36                                | 4.14   | 109                                       | $15.7 \pm 1.6 \pm 0.9$                  | $10.7 \pm 1.0 \pm 0.8$                      |
| 5.36 - 6.23                                | 4.93   | 110                                       | $11.1 \pm 1.1 \pm 0.7$                  | $12.0 \pm 1.1 \pm 0.9$                      |
| 6.2 - 7.3                                  | 5.9  | 106                                       | $8.31 \pm 0.86 \pm 0.49$                | $12.5 \pm 1.2 \pm 0.9$                      |
| 7.3 - 8.5                                  | 7.0  | 87  | $5.56 \pm 0.64 \pm 0.33$                | $12.2 \pm 1.3 \pm 0.9$                      |
| 8.5 - 10.1                                 | 8.4  | 98  | $5.16 \pm 0.57 \pm 0.30$                | $15.6 \pm 1.6 \pm 1.1$                      |
| 10.1 - 12.0                                | 10.1   | 108                                       | $3.70 \pm 0.38 \pm 0.22$                | $20.8 \pm 1.9 \pm 1.5$                      |
| 12.0 - 14.6                                | 12.3   | 82  | $2.12 \pm 0.26 \pm 0.12$                | $16.1 \pm 1.8 \pm 1.1$                      |
| 14.6 - 18.1                                | 15.3   | 64  | $1.39 \pm 0.19 \pm 0.08$                | $20.7 \pm 2.4 \pm 1.5$                      |
| 18.1 - 23.3                                | 19.6   | 56  | $0.67 \pm 0.10 \pm 0.04$                | $17.4 \pm 2.2 \pm 1.2$                      |
| 23.3 - 31.7                                | 26.2   | 42  | $0.251 \pm 0.041 \pm 0.015$             | $17.1 \pm 2.5 \pm 1.2$                      |
| 31.7 - 48.5                                | 38.0   | 36  | $0.127 \pm 0.023 \pm 0.007$             | $18.3 \pm 3.0 \pm 1.3$                      |
| 48.5 - 100.0                               | 67.4   | 22  | $0.0228 \pm 0.0072 \pm 0.0008$          | $17.7 \pm 4.8 \pm 0.8$                      |
| 100.0 - 180.0                              | 128.9  | 3   | $0.0036^{+0.0057}_{-0.0020} \pm 0.0002$ | $14^{+16}_{-10} \pm 1$                      |

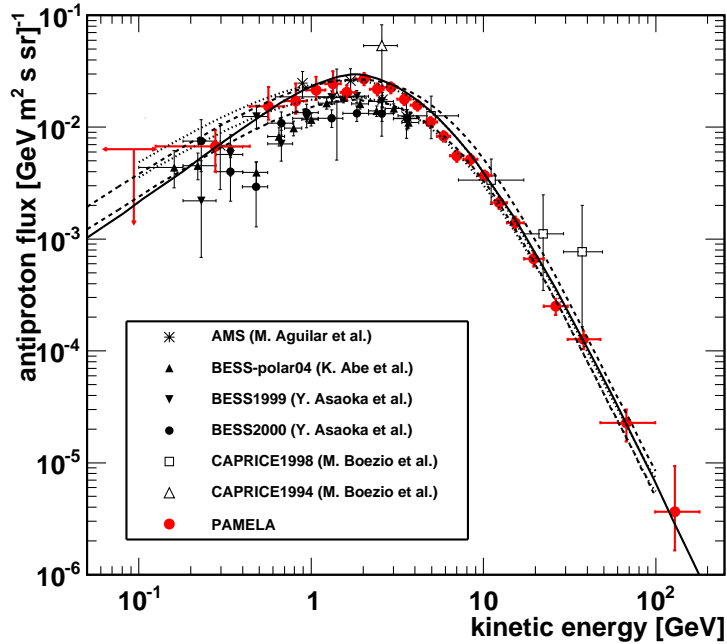


FIG. 1: The antiproton energy spectrum at the top of the payload obtained in this work compared with contemporary measurements [21–25] and theoretical calculations for a pure secondary production of antiprotons during the propagation of cosmic rays in the galaxy. The dotted and dashed lines indicate the upper and lower limits calculated by Donato et al. [26] for different diffusion models, including uncertainties on propagation parameters and antiproton production cross-sections, respectively. The solid line shows the calculation by Ptuskin et al. [27] for the case of a Plain Diffusion model.

measurements. Figure 3 shows the PAMELA antiproton-to-proton flux ratio compared with a calculation [14] (dashed line) including both a primary antiproton component from the annihilation of 180 GeV wino-like neutralinos and secondary antiprotons. This model, based on the non-thermal production of dark matter in the early universe, was proposed to explain the high-energy rise in the PAMELA positron fraction [8]. As shown by the dashed line in Figure 3, a reasonable choice of GALPROP [31] propagation parameters (dashed-dotted line) allows a good description of PAMELA antiproton data with the inclusion of the wino-annihilation signal. Given current uncertainties on propagation parameters, this primary component cannot be ruled out. It has also been suggested that the PAMELA positron data can be explained without invoking a primary component. This is possible if

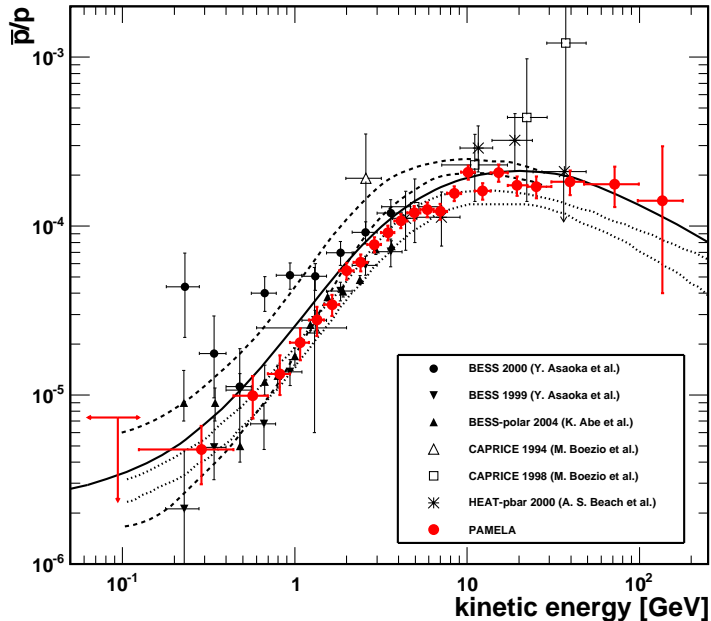


FIG. 2: The antiproton-to-proton flux ratio at the top of the payload obtained in this work compared with contemporary measurements [21–24, 28] and theoretical calculations for a pure secondary production of antiprotons during the propagation of cosmic rays in the galaxy. The dashed lines show the upper and lower limits calculated by Simon et al. [6] for the Leaky Box Model, while the dotted lines show the limits from Donato et al. [30] for a Diffusion Reacceleration with Convection model. The solid line shows the calculation by Ptuskin et al. [27] for the case of a Plain Diffusion model.

secondary production takes place in the same region where cosmic rays are being accelerated [11]. An increase in the antiproton [32] and secondary nuclei abundances [33] are also predicted in this model. The solid line in Figure 3 shows the prediction for the high-energy antiproton-to-proton flux ratio. While this theoretical prediction is in good agreement with the PAMELA data, in this energy region it does not differ significantly from the expectation for standard secondary production models. Comparisons with experimental secondary cosmic-ray nuclei data are needed along with higher energy antiproton measurements. New data on the boron-to-carbon ratio measured by PAMELA will soon become available, while the antiproton spectrum is likely to be probed at higher energies by AMS-02 experiment [34] which will soon be placed on the International Space Station.

We have measured the antiproton energy spectrum and the antiproton-to-proton flux ratio over the most extended energy range ever achieved and with no atmospheric overbur-

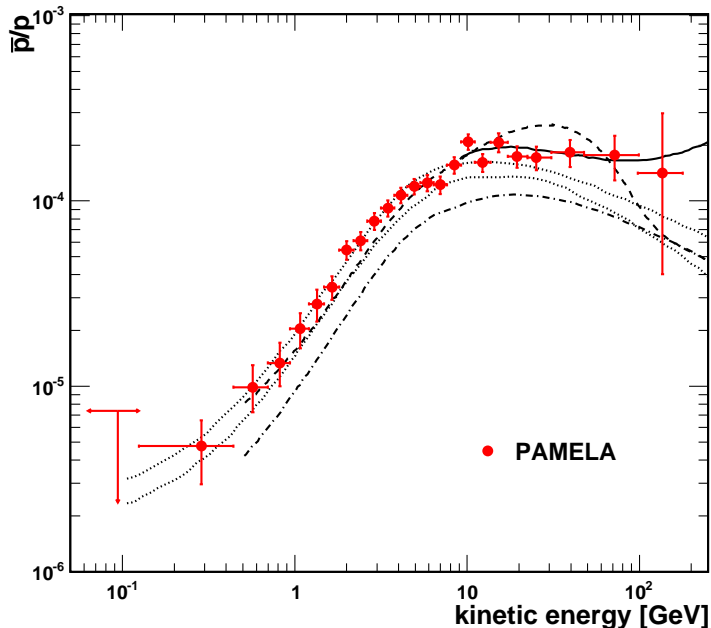


FIG. 3: The antiproton-to-proton flux ratio at the top of the payload obtained in this work compared with theoretical calculations. The dotted lines show the upper and lower limits calculated for a pure secondary production of antiprotons during the propagation of cosmic rays in the galaxy by Donato et al. [30] for a Diffusion Reacceleration with Convection model. The dashed line is a calculation by Kane et al. [14] including both a primary antiproton component from annihilation of 180 GeV wino-like neutralinos and secondary antiprotons (dashed-dotted line for the secondary component). The solid line show the calculation by Blasi and Serpico [32] for secondary antiprotons including an additional antiproton component produced and accelerated at cosmic-ray sources.

den. Our results are consistent with pure secondary production of antiprotons during the propagation of cosmic rays in the galaxy. We note that the quality of our data surpasses the current precision of the theoretical modeling of the cosmic-ray acceleration and propagation mechanisms. Improved models are needed to allow the full significance of these experimental results to be understood.

We acknowledge support from The Italian Space Agency (ASI), Deutsches Zentrum für Luft- und Raumfahrt (DLR), The Swedish National Space Board, The Swedish Research

Council, The Russian Space Agency (Roscosmos) and The Russian Foundation for Basic Research.

---

\* On leave from School of Mathematics and Physics, China University of Geosciences, CN-430074 Wuhan, China

- [1] G. Jungman, M. Kamionkowski, and K. Griest, *Phys. Rep.* **267**, 195 (1996).
- [2] L. Bergström, *Rep. Prog. Phys.* **63**, 793 (2000).
- [3] G. Bertone, D. Hooper, and J. Silk, *Phys. Rep.* **405**, 279 (2005).
- [4] S. Hawking, *Nature* **248**, 30 (1974).
- [5] P. Kiraly et al., *Nature* **293**, 120 (1981).
- [6] M. Simon, A. Molnar, and S. Roesler, *Astrophys. J.* **499**, 250 (1998).
- [7] O. Adriani et al., *Phys. Rev. Lett.* **102**, 051101 (2009).
- [8] O. Adriani et al., *Nature* **458**, 607 (2009).
- [9] O. Adriani et al., to appear on *Astropart. Phys.*, arXiv:1001.3522v1.
- [10] M. Boezio et al., *New J. Phys.* **11**, 105023 (2009).
- [11] P. Blasi, *Phys. Rev. Lett.* **103**, 051104 (2009).
- [12] M. Cirelli, M. Kadastik, M. Raidal, and A. Strumia, *Nucl. Phys. B* **813**, 1 (2008).
- [13] I. Cholis, G. Dobler, D. P. Finkbeiner, L. Goodenough, and N. Weiner, *Phys. Rev. D* **80**, 123518 (2009).
- [14] G. Kane, R. Lu, and S. Watson, *Phys. Lett. B* **681**, 151 (2009).
- [15] P. Picozza et al., *Astropart. Phys.* **27**, 296 (2007).
- [16] A. Bruno, Ph.D. thesis, University of Bari, Bari, Italy (2008), <http://pamela.roma2.infn.it/>.
- [17] R. Brun et al., Detector description and simulation tool, CERN program library (1994), version 3.21.
- [18] S. Straulino et al., *Nucl. Instrum. Meth. A* **556**, 100 (2006).
- [19] P. Hofverberg, Ph.D. thesis, Royal Institute of Technology (KTH), Stockholm, Sweden (2008), <http://pamela.roma2.infn.it/>.
- [20] J. Wu, Licentiate thesis, Royal Institute of Technology (KTH), Stockholm, Sweden (2010).
- [21] M. Boezio et al., *Astrophys. J.* **487**, 415 (1997).
- [22] M. Boezio et al., *Astrophys. J.* **561**, 787 (2001).

- [23] Y. Asaoka et al., Phys. Rev. Lett. **88**, 051101 (2002).
- [24] K. Abe et al., Phys. Lett. B **670**, 103 (2008).
- [25] M. Aguilar et al., Phys. Rep. **366**, 331 (2002).
- [26] F. Donato et al., Astrophys. J. **563**, 172 (2001).
- [27] V. S. Ptuskin et al., Astrophys. J. **642**, 902 (2006).
- [28] A. S. Beach et al., Phys. Rev. Lett. **87**, 271101 (2001).
- [29] L. J. Gleeson and W. I. Axford, Astrophys. J. **154**, 1011 (1968).
- [30] F. Donato, D. Maurin, P. Brun, T. Delahaye, and P. Salati, Phys. Rev. Lett. **102**, 071301 (2009).
- [31] A. W. Strong and I. V. Moskalenko, Astrophys. J. **509**, 212 (1998).
- [32] P. Blasi and P. D. Serpico, Phys. Rev. Lett. **103**, 081103 (2009).
- [33] P. Mertsch and S. Sarkar, Phys. Rev. Lett **103**, 081104 (2009).
- [34] R. Battiston et al., in Proc. 29th Int. Cosmic Ray Conf. (Pune) (2005), vol. 10, p. 151.
- [35] J. W. Bieber et al., Phys. Rev. Lett. **83**, 674 (1999).
- [36] U. W. Langner and M. S. Potgieter, Adv. Sp. Res. **34**, 144 (2004).
- [37] While more precise models of solar modulation, accounting for effects such as sign-charge dependence of the modulation, exist (e.g. [35, 36]), the force field model is a simple approach that provides a reasonably good approximation of the solar modulation above 1-2 GeV.